Experimental Study on Solid Circulation in a Multiple Jet Fluidized Bed

Gaurav Agarwal, Brian Lattimer, Srinath Ekkad, and Uri Vandsburger
Dept. of Mechanical Engineering, Virginia Tech, Blacksburg, VA 24061

DOI 10.1002/aic.13703
Published online December 2, 2011 in Wiley Online Library (wileyonlinelibrary.com).

Particle image velocimetry was used to investigate the evolution of multiple inlet gas jets located at the distributor base of a two-dimensional fluidized bed setup. Results were used to estimate the solid circulation rate of the fluidized bed as well as particle-entrainment into the individual jets. The effects of fluidization velocity, orifice diameter, orifice pitch, particle diameter, and particle density were studied. It was determined from this study that the solid circulation rate linearly increased with an increase in the fluidization velocity until the multiple jet system transitioned from isolated to an interacting system. In the interacting system of jets, the solid circulation increased with fluidization velocity but at a much lower rate. For multiple jet systems, this phenomenon may indicate the presence of an optimum operating condition with high circulation rate and low air input in the bed. © 2011 American Institute of Chemical Engineers *AIChE J,* 58: 3003–3015, 2012
Keywords: fluidization, multiple jets, particle image velocimetry, solid volume fraction, solid circulation, particle entrainment

Introduction

Fluidized beds commonly consist of multiple jets of oxygen containing gas located at the bottom of the bed to fluidize particulate media as well as support the combustion and gasification of solid fuel. The importance of these jets is reflected by their ability to act as a reacting medium and to control the reactors that produce syngas from gasification of fuels such as coal and biomass. These jets entrain gas and particles from the emulsion thereby enhancing the gas-particle mixing. Thus, the entrainment process helps to promote heat transfer, mass transfer, and chemical reaction rates for a fluidized bed reactor. For proper performance estimation, the patterns and extent of gas-particle mixing must be determined for a reactor. Failure to predict these factors may lead to problems such as particle agglomeration, temperature hot spots, and partial defluidization.

Various mathematical and empirical models for particle entrainment rate have been suggested in the literature. One of the earliest studies in this regard was done by Thorley et al.[1] using semicylindrical spouted beds. In the research conducted by Thorley et al.,[1] the forces acting on particles in the jet spout were balanced to estimate the particle velocity profile. Lefroy[2] suggested an alternative approach to predict the solid circulation rate by solving mass and momentum equations for bed voidage and particle velocities in the jet spout. This approach was further supplemented by various works in the literature.[3–7] Van Deemter[8] developed the counter-current flow model for gas–solid fluidized beds to propose the bubble induced particle mixing and solid circulation. This was further extended by Baeyens et al.[9] and van Deemter[10] into comprehensive models and empirical equations to estimate the model parameters, particle velocities, circulation flux, bed turnover time, gas back mixing, residence time, segregation, and defluidization. Merry[11] developed a particle entrainment model based on particle stream function and validated it experimentally using a liquid–solid fluidized bed. Donsi et al.[12] developed a mathematical model based on the turbulent jet theory[13] to describe the observed jet characteristics in a two-dimensional bed. This was further extended by Massimilla[14] to a more detailed model which included mode of discharge, jetting regions, penetration depths, expansion angle, entrainment, bubble size and transport models. Further computational studies were conducted by various researchers to understand the influence of solid circulation on bed dynamics.[5,10–14]

Various experimental studies have been performed to provide the empirical input parameters for these mathematical models, as well as to provide the data for model validation.[3,15,16] The most important parameters to quantify the particle entrainment rate are particle velocities and void fraction values. These parameters are estimated either inside the jet or along the jet periphery. Several intrusive and non intrusive techniques have been applied to quantify these parameters in experimental fluidized beds setups. Some of these techniques include photographs and visual analysis,[1,11,12,17–20] pitot tubes,[12,18,21] fiber optic probes,[4,22–27] tracer particles,[7,21,28,29] tracer gas,[19,30] gamma-ray densitometer,[15,31] positron emission particle tracking,[32,33] x-ray tomography,[34,35] digital image analysis,[36–39] and particle-image velocimetry (PIV).[40,41] Most of these experimental studies have been conducted using single jet spouted beds. Also, reports on the influence of multiple jet systems on solid circulation are still sparse in the literature.

Correspondence concerning this article should be addressed to G. Agarwal at gauravag@vt.edu.

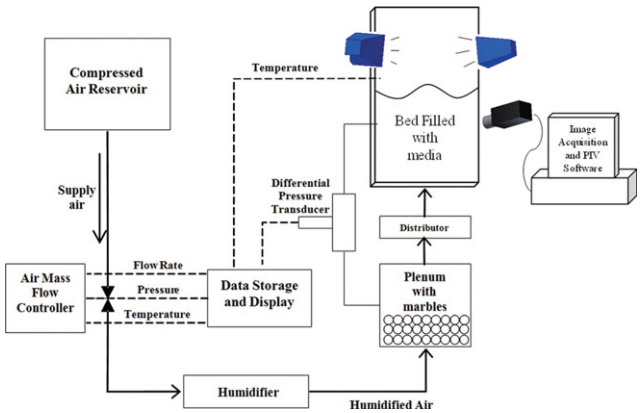

Figure 1. Schematic of experimental setup.

[Color figure can be viewed in the online issue, which is available at wileyonlinelibrary.com.]

The motivation behind this study was to understand the effect of distributor orifice diameter, orifice pitch, particle types, and operating conditions on the solid circulation dynamics of a multiple jet system fluidized bed. PIV has recently been used on a single jet system to analyze the solid circulation behavior.[40] However, its application onto multiple jet systems has not been reported in the literature. In this study, PIV and a two-dimensional bed were used to visualize and analyze the solid circulation phenomena, including jet entrainment, on a multiple jet system.

Experimental

Experimental setup

A two-dimensional fluidized bed setup of dimensions 0.76 m high and 0.25 m wide was used in this research. Figure 1 contains a schematic of the experimental setup. The thickness of the bed was 0.0127 m to ensure that the ratio of bed thickness to particle diameter is greater than 10 to avoid particle bridging effects.[42,43] The bed walls were made of high optical clarity glass, and a light absorbing black sheet was located on the back side. The bed was illuminated homogeneously using two halogen lamps of 500 W each, which were located approximately at a 45° angle from the bed axis. A Flowsense MKII (4 Megapixel) PIV camera was used to take double frame digital images of the bed. The camera was controlled through a timer box, and images were stored and processed in a computer using Dynamic Studio 3.0 software. The setup was surrounded by black barriers and curtains to avoid reflections in captured images.

Air supply was controlled through a 500 SLPM ALICAT (Model No. MCR-500SLPM-D/10M) mass flow controller (accuracy: ±0.4% reading, +0.2% FS). As shown in Figure 1, the air was channeled through a humidifier to avoid electrostatic effects in the bed. The water content of the humidifier was kept to a minimum to avoid saturation. Air was then fed into the plenum chamber and injected into the bed through a perforated plate distributor. The plenum was filled with marbles to ensure uniform fluidization. A Setra (Model no. 264) differential pressure transducer (ranging 0–25,000 Pa, accuracy ±0.25% FS) was used to measure the pressure drop between the plenum and the freeboard. Differential pressure, inlet pressure, inlet temperature and air flow rate data were recorded using a National Instruments data acquisition system.

Table 1. Physical Properties of Tested Fluidized Bed Media

Particle	d_p (μm)	ρ_p (kg/m^3)	U_{mf} (m/s)	Geldart Group
Glass	550	2500	0.22	B
Glass	750	2500	0.35	D
Ceramic	550	1079	0.20	B

Table 2. Description of Perforated Distributor Plates

Distributor Type	d_o (mm)	N (Number of Holes)	P (m)
A1	2	9	0.028
A2	2	5	0.056
B1	3	4	0.063

Test cases

Test cases were developed to explore the effect of changing particle size, particle density, fluidization velocity, orifice diameter and orifice pitch on the solid circulation behavior. Three types of particles were selected to provide diameter ranging 550–750 μm and density ranging 1079–2500 kg/m^3. As listed in Table 1, this resulted in particles with Geldart B and D classification. Ceramic 550 μm and glass 550 μm particles have the same mean diameter, different density, and the same Geldart B classification. Glass 550 μm and glass 750 μm particles differ in mean diameter and Geldart classification but have same density. The particles were sieved through calibrated sieves multiple times within 100 μm range. The particle-size distribution was assumed to be normal and the mean diameter is reported in Table 1. Each type of particle was examined using three different types of perforated distributor plates. As listed in Table 2, effects of orifice diameter and orifice pitch were evaluated in this study. Distributor Type A1 and A2 have same orifice diameter but different orifice pitch. Distributor Types A and B differ in orifice diameter. Distributor Type A1 and B1 were designed to have the same total orifice flow area. Thus, at same superficial velocity for Type A1 and B1 distributors, the effect of orifice diameter can be compared at the same orifice velocity. The uncertainty in orifice diameter was within ±0.02 mm to ensure the flow rate uniformity. The periphery of the orifices is shown in Figure 2 to be located 1.59 mm from the bed wall aiding in the optical assessment of jets. Similar orifice arrangements have been used for optical assessment

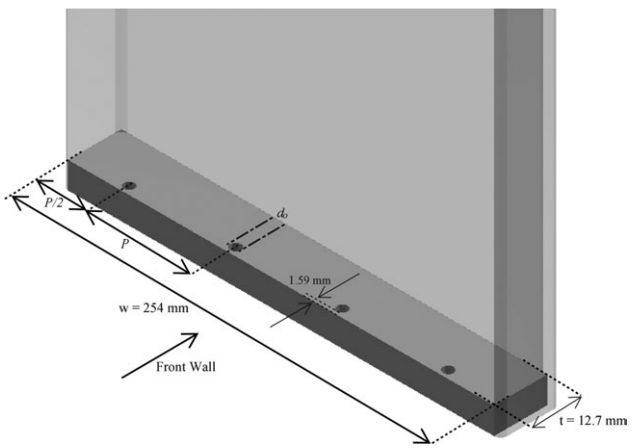

Figure 2. Schematic of distributor plate.

Table 3. Comparison of Experimental Minimum Fluidization Velocities Measured for Cylindrical and Two-Dimensional Bed Test Runs

Distributor Type	Glass 550 μm Particles (m/s)	Glass 750 μm Particles (m/s)	Ceramic 550 μm Particles (m/s)
3D Bed[a]	0.22	0.35	0.20
A1[b]	0.23 [1.0]	0.34 [1.0]	0.23 [1.1]
A2[b]	0.21 [0.9]	0.28 [0.8]	0.17 [0.9]
B1[b]	0.23 [1.0]	0.34 [1.0]	0.18 [0.9]

Term in bracket indicates $U_{mf,2D}/U_{mf,3D}$ for the corresponding particle type.
[a]$U_{mf,3D}$ (m/s).
[b]$U_{mf,2D}$ (m/s).

of jet characteristics in two-dimensional and semicylindrical beds with a flat front wall.[12,17,21,44–50]

Recent review articles have cautioned the application of two-dimensional fluidized bed data for quantitatively predicting cylindrical fluidized beds.[42,43] However, it was acknowledged that the two-dimensional beds provide qualitative and semiquantitative indications of behavior for an axis-symmetric cylindrical column. It has also been recommended[42,43] to keep the ratio of bed thickness to particle diameter high (aprroximately10–20) to avoid any particle bridging effects in a two-dimensional fluidized bed setup. In absence of such conditions, frictional resistance becomes a dominant force in restraining the particle motion along the front and rear faces of the bed.[43] In the current study, the ratio of bed thickness to particle diameter was kept at 23 for glass and ceramic 550 μm particles and 17 for glass 750 μm particles.

Analysis Procedure

Pressure drop analysis

The differential pressure drop was analyzed to calculate the minimum fluidization velocity ($U_{mf,2D}$) for each combination of particle type and distributor type in the two-dimensional bed. These velocities are listed in Table 3 and compared with minimum fluidization velocities ($U_{mf,3D}$) calculated for respective particles in a cylindrical fluidized bed setup.[51] Experimental data was taken starting with the bed at the maximum flow rate, which was approximately two times the minimum fluidization velocity. The flow rate was decreased by 5 SLPM and then held constant for 300 s before the data acquisition.

Particle image velocimetry

PIV is a nonintrusive optical technique used to quantify velocity field information of seeding particles suspended in a fluid through measurement of particle displacement over a known time interval. Due to dense media prohibiting laser passage in the bed, a conventional PIV technique cannot be used to obtain gas or particle velocities. However, PIV can be used to quantify particle velocities near the front wall. Hence, the bed was homogenously illuminated using halogen lights and bed media was used as seeding particles to quantify the particle velocity field.

The camera was located at a distance of 1.0 m from the front wall which enabled a field-of-view covering the full width and expanded height of the bed. Magnification factor of this setup ensures that each particle occupies approximately 3–4 pixels on a CCD frame of the 4 Megapixel PIV camera. Measurements at each flow rate included 25 double frame images taken at a trigger rate of 7.4 Hz. This resulted in measuring the flow field over 3.38 s. The time delay between each pair of double frame images was 1 ms. An adaptive correlation technique was applied where the interrogation area (IA) for each reading was iteratively reduced from 128 × 128 pixels to 32 × 32 pixels in two steps. The relative overlap of 25% and the peak validation of 1.2 were applied for PIV analysis. A sample PIV mean superimposed onto the mean image is shown in Figure 3. PIV vectors inside the jet were masked, as the time delay was set to get better velocity profiles in the annulus area outside the jets.

Solid volume fraction analysis procedure

Quantifying the solid volume fraction, ε_s, of a fluidized bed is necessary to investigate its hydrodynamics. In two-dimensional fluidized beds, the images of fluidizing particles can be obtained at the bed front wall. The time average intensity analysis of these images can be used to determine the solid volume fraction in a two-dimensional bed.[36,38,39,52–54] This section discusses the procedure used to determine the solid volume fraction values for the bed.

Corrected Intensity Maps. Twelve bit images were captured in these experiments, ranging the pixel intensity level from 0 (for dark regions) to 4095 (for bright regions) for a window of 2048 × 2048 pixels. Fluidizing bed images were subtracted by a base image to obtain a homogenously lit image. The base image was taken without any particles in the bed to remove the illumination irregularities. The resultant image intensities were then scaled from 0 (absolute gas phase) to 1 (particulate phase). This scaling ensured that different type particles (glass or ceramic) with varying spectral properties are equally treated mathematically. Thereafter, the scaled intensity of each pixel was spatially averaged for the same size as the PIV vector Interrogation Area (IA). This enabled each of the 85 × 85 PIV velocity vectors in the image window to have a corresponding averaged intensity value. Lastly, the images taken at different air flow rates were linearly corrected using the intensity difference caused by the level of smearing in those images due to moving particles to get the corrected intensity, I_{cor}, for each IA. This image analysis is shown for an instantaneous image in Figure 4. The image processing work was performed using MATLAB 7.9 (R2009b).

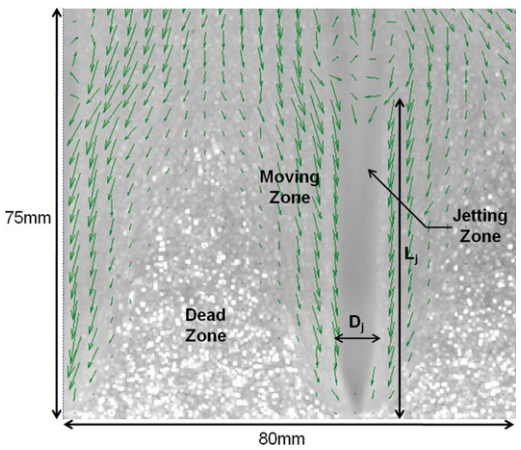

Figure 3. Jet at the bottom of Type A2 distributor plate using glass 550 μm particles: PIV mean superimposed onto mean image of acquired images.

[Color figure can be viewed in the online issue, which is available at wileyonlinelibrary.com.]

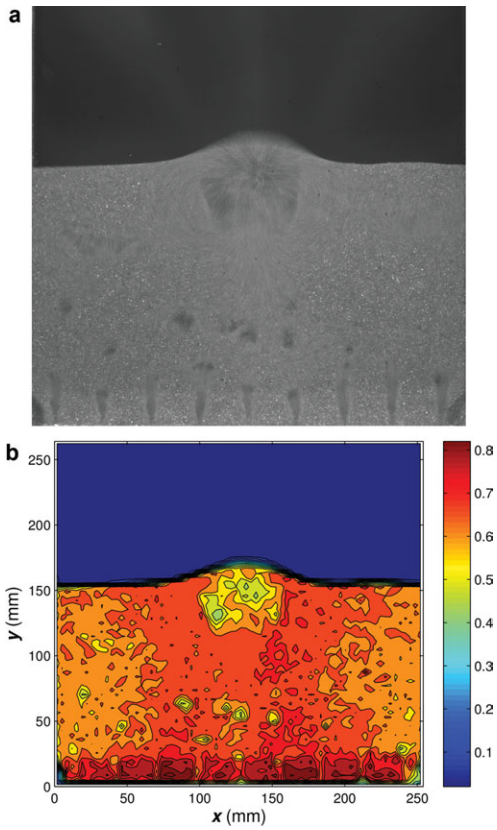

Figure 4. Image analysis for the test case of glass 550 μm particles using Type A1 distributor at U_f = 0.31 m/s: (a) Instantaneous image with non-homogenous illumination (b) Corrected intensity, I_{cor}, map of the instantaneous image.

0 represents all gas and 1 represents all particulate phase. [Color figure can be viewed in the online issue, which is available at wileyonlinelibrary.com.]

Bulk Solid Fraction. The bulk solid volume fraction, $\varepsilon_{s,b}$, of the fluidized bed was calculated at a set fluidization velocity to develop a solid volume fraction correlation based on I_{cor} of the respective IAs. For this purpose, the corrected intensity, I_{cor}, maps were time-averaged for the data acquisition period of 3.38 s. These time-averaged I_{cor} maps were used to quantify the bulk solid volume fraction, $\varepsilon_{s,b}$, of the bed at a set air flow rate. First, the time-averaged I_{cor} intensity value was averaged along the bed width and plotted along the height above distributor, as shown in Figure 5a. The bed expansion height was the vertical location at which this intensity is 5% of the maximum value (1.0). The calculated bed expansion height was subsequently used to determine the $\varepsilon_{s,b}$ using the known bed mass, as shown in Figure 5b.

Solid Volume Fraction. The time-averaged I_{cor} value for each interrogation area was converted to the mean solid volume fraction, ε_s, along the thickness of the bed using the following correlation.

$$\varepsilon_s = (AI_{cor})^B \tag{1}$$

The term AI_{cor} represents the area fraction occupied by illuminated particles on the front wall of the fluidized bed. This includes higher intensity particles at the front wall and lower intensity particles along the thickness of the bed. The basis for the assumption that the measured intensity represents the particle area fraction came from the studies conducted by Heffels et al.[55] and Boerefjin et al.,[53] in which they concluded that the backscattered light reflected from the particle suspensions is an indication of the total reflecting surface area of the particles. A similar conclusion was made by Poletto et al.[52] using image analysis on a water fluidized bed of $3d_p$ bed thickness.

The parameter B was introduced in Eq. 1 to convert this area fraction to mean solid volume fraction, ε_s, along the thickness of the bed. This was followed by the work of Link et al.,[36,37] where porous cube theory was applied onto two-dimensional fluidized beds to obtain a correlation between its intensity and solid volume fraction

$$\varepsilon_s = (I_m)^{1.5} \tag{2}$$

In the correlation proposed by Link et al. in Eq. 2, I_m represents the area fraction of particles on the front wall computed through intensity manipulation, which is similar to AI_{cor} term in Eq. 1 with $A = 1$. I_m was raised by a power of 1.5 to obtain mean ε_s along their bed thickness ($6d_p$). This

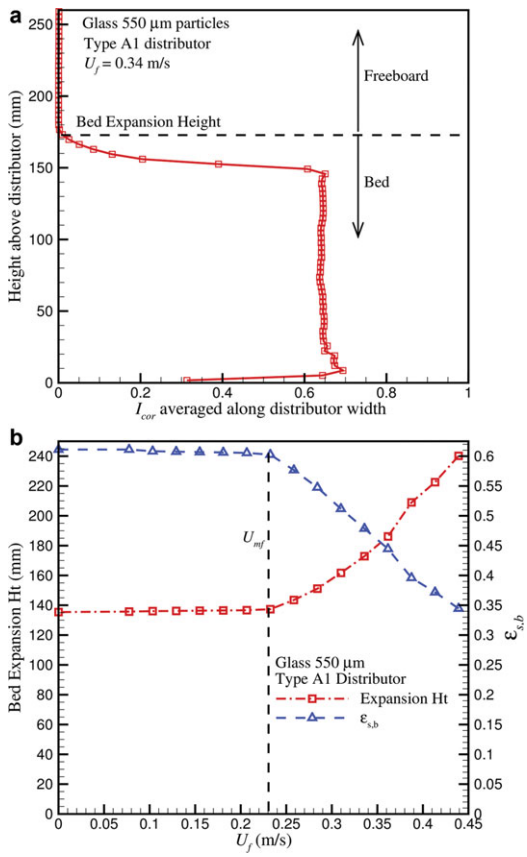

Figure 5. Bulk solid volume fraction, $\varepsilon_{s,b}$, estimation for glass 550 μm particles using Type A1 distributor.

Bed mass is 0.6674 kg: (a) Corrected Intensity averaged along distributor width vs. height above distributor at U_f = 0.35 m/s (b) Bed expansion height and $\varepsilon_{s,b}$ for bed superficial velocities. [Color figure can be viewed in the online issue, which is available at wileyonlinelibrary.com.]

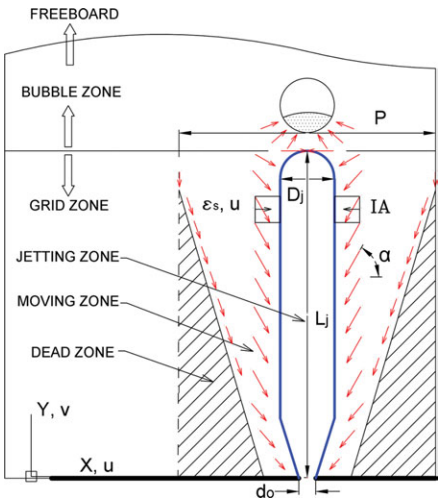

Figure 6. Phenomenological model for jets in two-dimensional beds.

IA selected along jet boundary is used to estimate particle entrainment rate. Horizontal velocity and ε_s were averaged from both sides of the jet boundary. [Color figure can be viewed in the online issue, which is available at wileyonlinelibrary.com.]

procedure was further validated using discrete particle model simulations.[36,37,39]

The values of A and B in Eq. 1 were empirically determined in this study. This was done by plotting the bulk solid fraction, $\varepsilon_{s,b}$, calculated as observed in the previous section with the time-averaged and the expanded bed dimension averaged I_{cor} values for varying fluidization velocities. Using a best fit to the data, the values for A and B were determined for each particle type. These A and B constants were subsequently used to quantify the solid fraction distribution, ε_s, using Eq. 1. The values of measured constants A and B are mentioned and discussed in later sections.

Particle entrainment and solid circulation

The jet boundary was determined to be linearly expanding from the orifice to the maximum diameter, as shown in Figure 6. Above this, the jet diameter remains constant until the bubble generates at jet tip.[56] Particle velocity vectors $\overrightarrow{u}$ and $\overrightarrow{v}$ of each IA were multiplied with their respective ε_s and particle density, ρ_p, to calculate horizontal and vertical particle mass fluxes ($\dot{m}''_x$ and $\dot{m}''_y$), respectively. The $\dot{m}''_x$, calculated along the jet boundary was multiplied with the jet surface area to obtain the particle entrainment rate for individual jets, $\dot{m}_{x,j}$. The jet surface area was calculated assuming the jet structure to be of a semicircular cross-section along the front wall. The jet diameter was always found to be lower than the thickness of the bed.[56] The expansion angle for each jet was calculated[56] to accurately determine the jet boundary and estimate the proposed jet surface area. The particle entrainment values were added for each jet to get the total solid circulation rate of the bed, $\dot{m}_{x,tot} = \sum_{j=1}^{N} \dot{m}_{x,j}$, at a set air flow rate. This procedure was used to estimate the solid circulation rate and particle entrainment rates for each fluidization velocity of the nine test cases using a MATLAB code.

Results and Discussion

The fluidized bed behavior was investigated while varying the operating parameters such as fluidization velocity, particle density, particle diameter, orifice diameter, and orifice pitch. A phenomenological model was developed to study the effect of these parameters on the geometrical characteristics of the jets and grid-zone behavior.[56] This section briefly describes the major characteristics of fluidized beds and then presents results on the patterns of solid fraction and solid circulation in a fluidized bed.

General bed fluidization characteristics

The grid-zone region of fluidized bed is shown in Figure 6 to be divided into three sub zones: particle moving zone, dead zone and jetting zone.[4,17,56,57] Figures 7a, b contains time averaged PIV and Prewitt filtered images for the fluidized bed at different fluidization velocities with glass 550 μm particles using Type B1 distributor plate.

Jet profiles can be classified into three systems: isolated, transitional and interacting, based on whether the respective moving zones of jets are interacting with the adjacent moving zones.[45,56] Jet systems were defined to be isolated if the moving zone of the adjacent jets did not mix with each other, as seen in Figure 7a. In a similar way, interacting jet systems were observed when all the jets in the system have moving zones that intermix with adjacent ones, as seen in Figure 7b. In transitional jet systems, some jets behaved as isolated while others had moving zones that intermix with adjacent ones. The occurrence of these three systems was dependent on fluidization velocity, pitch of orifice and particle properties.

A permanent jet shape was found in all test cases. This is consistent with the criteria proposed by Grace and Lim[58] where permanent jet formation is expected when $d_o/d_p \leq 25.4$. Rowe et al.[59] attributed this finding to the presence of wall structures in two-dimensional bed in comparison to his study done on a cylindrical bed where they found a stream of bubbles instead. This phenomena was verified in a recent study as well.[60]

Solid volume fraction results

Figure 8a contains the plot of $\varepsilon_{s,b}$ along with time-averaged and expanded bed dimension averaged I_{cor}. A least-square fit to the $\varepsilon_{s,b}$ data using the Eq. 1 is also plotted for the corresponding fluidization velocity test case. The constants A and B values were found close to the values reported by Link et al.,[36] with constant B value being close to 1.42 for all three particles types and constant A varying around 1.0 with some dependence on particle type and size.

It is thus concluded that in Eq. 1, A represents the spectral parameter of the fluidized particles. This parameter converts the corrected intensity to the area fraction occupied by particles on the front wall. For the particles that reflect the intensity equivalent to its projected area, the value of A should be close to 1. For particles that reflect more light than its corresponding projected area, the parameter A would be lower than 1 to convert particle intensity to its correct projected area. This was observed for ceramic 550 μm particles with A being 0.82. Similarly, A would be higher than 1 for particles reflecting less light than its corresponding projected area. The parameter B converts the projected particle area fraction to the mean solid volume fraction, ε_s, along the thickness of the bed. Thinner beds would tend to have B closer to 1 as observed in results of Poletto et al.[52] and Boerefjin et al.[53] Beds with higher thickness to particle diameter ratio would tend to have B higher than 1, as observed in the current experimental results and those of Link et al.[36]

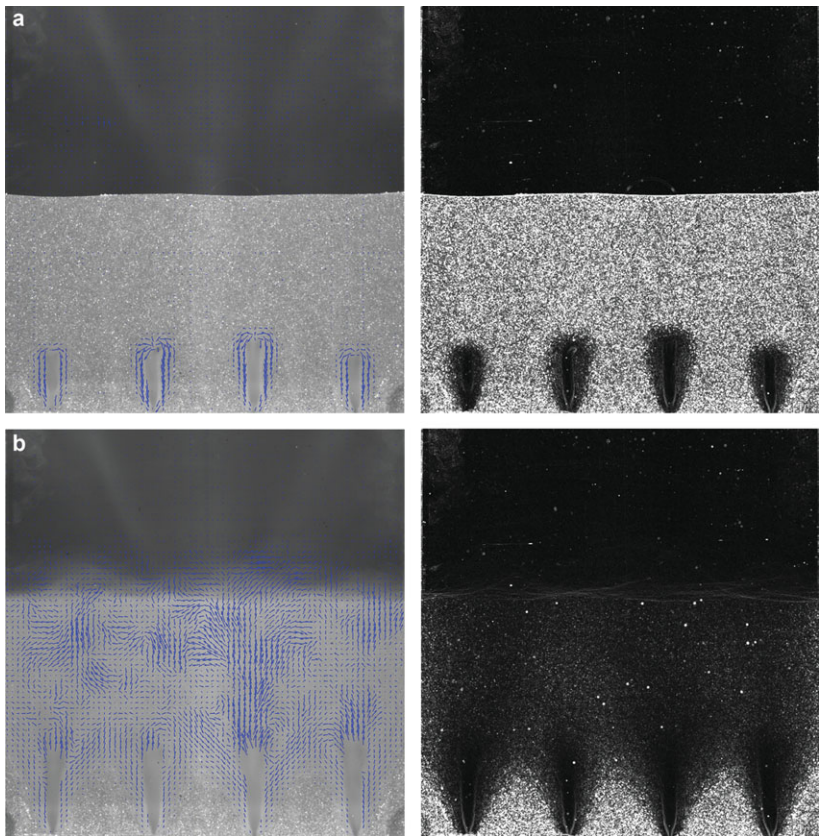

Figure 7. PIV data superimposed on mean image of acquired images, and Prewitt filter applied on mean image.

Test-case of Type B1 distributor using glass 550 μm particles exhibiting different jet systems (a) $U_f/U_{mf,2D} = 1.12$, isolated system and (b) $U_f/U_{mf,2D} = 1.46$, interacting system. Field of view is 250 mm wide by 200 mm high. [Color figure can be viewed in the online issue, which is available at wileyonlinelibrary.com.]

Figure 8b provides the plot for absolute error in total bed mass calculated using the solid fraction model, Eq. 1, against the actual mass of particles fluidized in the bed. This error was found to be less than 15% for all nine test cases at varying fluidization velocities. Figure 8c contains the void fraction map ($\varepsilon_f = 1-\varepsilon_s$), calculated using Eq. 1, for the instantaneous image shown in Figure 4a.

Figure 9a contains the plot of solid volume fraction profile along the jet boundary (a-b-c), including the conical bottom, for ceramic 550 μm particles using Type A1 distributor plate at $U_f/U_{mf,2D} = 1.46$. The solid fraction values increase almost linearly along the cone length to attain its maximum value at the location where conical part of the jet structure ends (a-b). This indicates the presence of dead zones in the vicinity of conical regions. Lower solid fraction near the bottom part of the jet is attributed to higher diffusion rate of high velocity gas from the jet into the bed. Further upwards along the jet height (b-c), the solid fraction profile gradually decreases along the constant diameter part of the jet indicating the influence of the particle moving zone on the solid fraction values. Figure 9a also contains the solid volume fraction profile along the center of jet 2 (p-q). The solid fraction values at the center are lower in comparison to the values at the boundary of the corresponding jet. The solid fraction values at the center follow the profile similar to that at the boundary, except for the upper part of the jet where a gradual increase in solid fraction was measured. This complements the observation at the jet boundary where the entrainment of particles leading to the decrease of solid fraction values now contributes to the increase of solid fraction values at the center of jet. Similar results were observed for other test cases involving different distributor types and particle combinations.

The profiles shown in Figure 9a match qualitatively with the theoretical results of Donsi et al.[12] for solid fraction values along the jet central axis, and computational results of Ettehadieh et al.[5] for solid fraction values 2.5 mm off the jet central axis. Quantitatively, the solid fraction values measured by Donsi et al.[12] and Ettehadieh et al.[5] were lower than those observed in Figure 9a. The reason for this difference could partially be attributed to mean jet orifice velocity, U_o, in the aforementioned studies being $\sim$2 times higher than the current study. Another comprehensive experimental study conducted by the same researchers,[15] using rectangular slit distributors and comparable inlet jet velocities revealed the solid volume fraction values to be in the same range as observed within the current study.

Figure 9b contains solid volume fraction profiles at different horizontal positions along the height of jet. As expected, the solid fraction values at the center of the jet are lower than those at the jet boundary and further lower than those located within the dead zone ($x/P = \pm 0.5$). The solid fraction profile at the jet center follows the same pattern as shown for the second jet in Figure 9a. The solid fraction value at the center is highest at $y = 0.010$ m and it gradually increases along the jet height from $y = 0.020$ m to $y = 0.060$ m. At the height of $y = 0.060$ m, the solid fraction values are almost uniform along the pitch of the distributor indicating the end of the jet length. The solid fraction values at the two jet boundaries are averaged and represented in Figure 9a. This

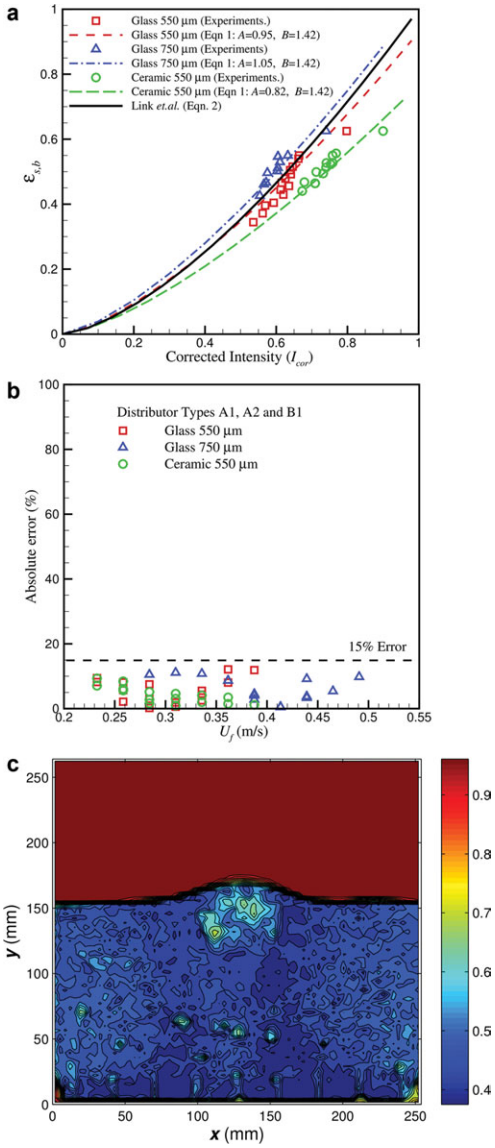

Figure 8. Validation and application of solid volume fraction correlation.

(a) Comparison of ε_s correlation (Eq. 1) with correlation from Eq. 2 and $\varepsilon_{s,b}$ values for different test cases. (b) Absolute error between actual bed mass and the mass calculated using ε_s correlation (Eq. 1) along the expanded bed dimensions (c) Void fraction ($\varepsilon_f = 1 - \varepsilon_s$) map calculated using Eq. 1 for the instantaneous image shown in Figure 4. [Color figure can be viewed in the online issue, which is available at wileyonlinelibrary.com.]

average value decreases slightly for height greater than 0.020 m due to the entrainment of particles from the moving zone into the jetting zone. The solid fraction values at the center of dead zones ($x/P = \pm 0.5$) do not show any change along the jet length for heights greater than 0.020 m. This horizontal profile of solid volume fraction was found to be similar to those seen in the literature.[61]

Particle entrainment and solid circulation

This section reviews the effect of variations in fluidization velocity, particle properties and distributor types on solid circulation and particle entrainment rates.

Fluidization Velocity. Figure 10a provides a plot of solid circulation rate for three particle types using the Type A1 distributor. Solid circulation was found to increase linearly with an increase in fluidization velocity until the jet systems transitioned from isolated to interacting jets. For the interacting jet systems, the rate of increase of solid circulation suddenly decreased in comparison to isolated jet systems. Although the linear increase of solid circulation with fluidization velocity has been observed in previous studies,[20,21,28,29] the sudden change in the rate of solid circulation has not been reported in the literature due to the lack of multiple jet studies. The relative leveling of solid circulation rate with fluidization velocity indicates that an optimum operating condition may exist for the applications that require high solid circulation for lower air input flow rate.

The accuracy of these solid circulation rate values were evaluated by comparing them with an alternate method presented by van Deemter.[8] The circulation rate was proposed to be calculated using a counter-current model developed for gas–solid fluidized beds[62,6,3]

$$\dot{m}_{x,\mathrm{tot}} = \rho_p \times (\varepsilon_{s,b}) \times (fr_{\mathrm{neg}}) \times (|v_{\mathrm{neg,avg}}|) \times (A_d) \qquad (3)$$

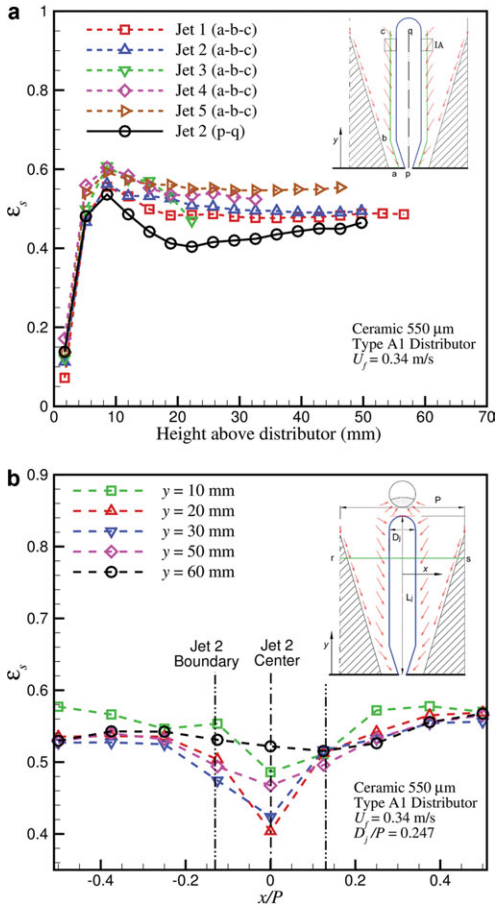

Figure 9. Solid volume fraction profiles for ceramic 550 µm particles with Type A1 distributor and U_f = 0.34 m/s.

(a) Solid volume fraction profile measured along jet boundary (a-b-c) and jet center (p-q) vs. height above distributor. Plot shows jet boundary data for five jets counting from left to right and jet center data for second orifice from the left. (b) Solid volume fraction profile for different horizontal locations (r-s) centered on the second jet from the left. [Color figure can be viewed in the online issue, which is available at wileyonlinelibrary.com.]

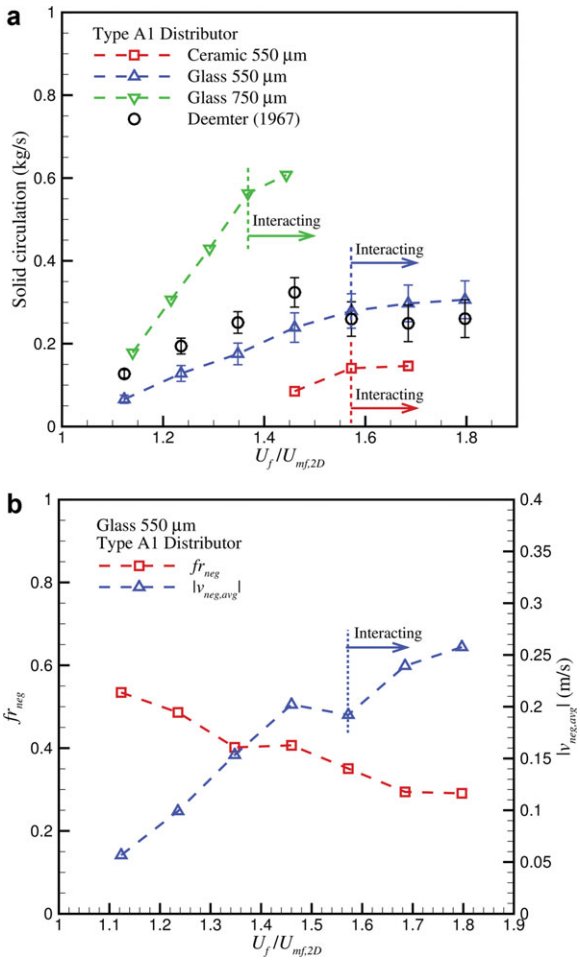

Figure 10. Analysis of solid circulation rate with change in fluidization velocity.

(a) Solid circulation rate calculated for the three particle types using Type A1 distributor vs. $U_f/U_{mf,2D}$. (b) fr_{neg} and $|v_{neg,avg}|$ calculated for glass 550 μm particles using Type A1 distributor vs. $U_f/U_{mf,2D}$. [Color figure can be viewed in the online issue, which is available at wileyonlinelibrary.com.]

In Eq. 3, $\varepsilon_{s,b}$ represents the bulk sold volume fraction calculated by Eq. 1, fr_{neg} represents the fraction of dense bed moving downwards, $|v_{neg,avg}|$ represents the average negative particle velocity of the bed, and A_d represents the cross-sectional distributor area. These parameters were calculated for the test-case of glass 550 μm particles using the Type A1 distributor plate at different fluidization velocities. The calculated solid circulation rates are plotted in Figure 10a along with the average uncertainty estimation of $\pm$18.2%. These circulation rate values are close in comparison to the values calculated using the method suggested in the current study, for which the average uncertainty was estimated to be $\pm$14.9%. As observed from Figure 10a, the values calculated by Eq. 3 overestimated the current results for isolated/transitional jet systems and under predicted values for the interacting jet systems.

It must be noted that the PIV camera settings were adjusted to get better signal/noise ratio for particle velocities participating in the jet entrainment. Particle velocities near the top of the bed are higher due to the eruption of bubbles.[64,65] This might lead to under prediction of $|v_{neg,avg}|$ using the current experimental settings, especially at higher fluidization velocity. Also, there is a level of unaccounted error within the estimation of fr_{neg} which is more accurately noted as the fraction of downward moving particle and interstitial gases.[10] It was not possible to accurately implement this definition onto the current results of the experimental study. However, the comparison between the data presented in Figure 10a shows reasonable agreement in solid circulation rate values calculated using the two methods. Figure 10b shows the parameters fr_{neg} and $|v_{neg,avg}|$ estimated for the discussed test-case. As noted, the fr_{neg} values were found to monotonically decrease with the increase in fluidization velocity. This trend can be partially explained on the basis of reduction of the dead zone areas and more particles participating in the fluidization of the bed due to the high velocity upward jets. The $|v_{neg,avg}|$ values were found to linearly increase with an increase in fluidization velocity, until the jet systems transitioned to interacting jets. For the interacting jet systems, a sudden decrease in $|v_{neg,avg}|$ values was observed which is consistent with the leveling of solid circulation rate observed in Figure 10a.

It was found that the major factor contributing to the leveling of solid circulation rate, calculated by the current experimental scheme, was the leveling of the horizontal particle entrainment velocity, $\overrightarrow{u}$, for the interacting jet systems. Figure 11 contains a plot of average entrainment velocities, U_{avg}, for the three test cases mentioned in Figure 10. U_{avg} was calculated while measuring the horizontal entrainment velocities along the jet boundaries and then averaging these values for all jets at a particular air flow rate, as shown in Figure 6. As observed from the Figure 11, U_{avg} increased linearly with the fluidization velocity until the jet systems transitioned to the interacting system, where U_{avg} started to level off. Since the jet length and jet diameter increased with fluidization velocity,[56] the leveling of horizontal entrainment velocities was the determining factor in the leveling off of the solid circulation rate.

Figure 12 provides the particle entrainment rate for each of nine individual jets with glass 550 μm particles and Type A1 distributor plate. It was observed that the particle entrainment in each jet is not same at a particular fluidization velocity. This difference in particle entrainment is primarily

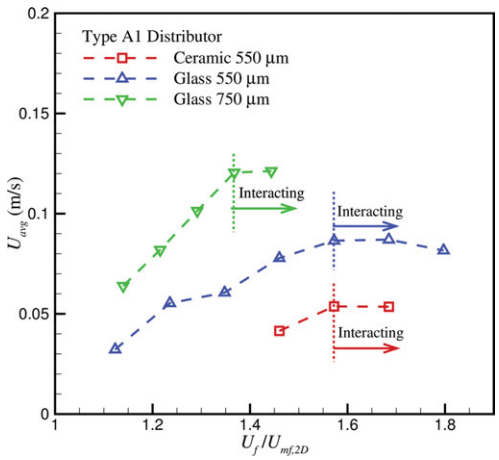

Figure 11. Average entrainment velocity, U_{avg}, vs. $U_f/U_{mf,2D}$ for three particle types using Type A1 distributor.

[Color figure can be viewed in the online issue, which is available at wileyonlinelibrary.com.]

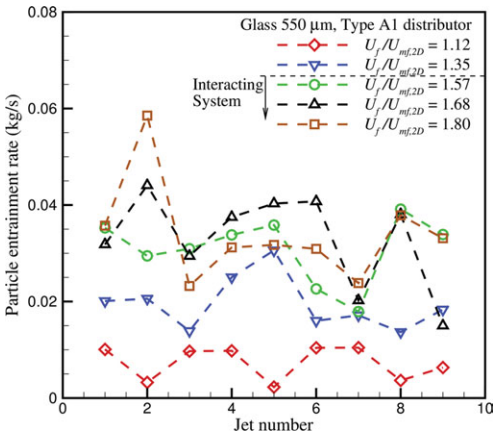

Figure 12. Particle entrainment for individual jets with glass 550 μm particles and Type A1 distributor plate.

Plot shows data for all 9 jets counting from left to right along the distributor width. [Color figure can be viewed in the online issue, which is available at wileyonlinelibrary.com.]

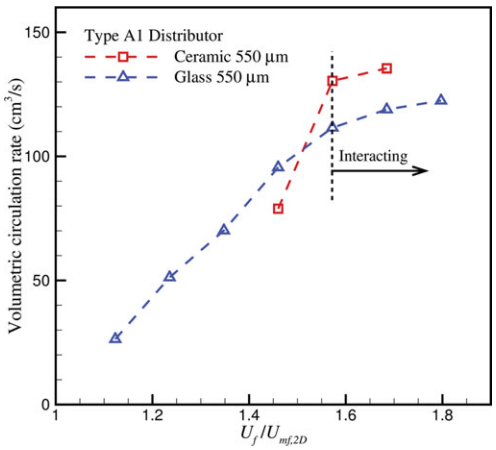

Figure 13. Volumetric circulation rate vs. $U_f/U_{mf,2D}$ for glass 550 μm and ceramic 550 μm particles using Type A1 distributor plate.

[Color figure can be viewed in the online issue, which is available at wileyonlinelibrary.com.]

attributed to differences in jet lengths and entrainment velocities for each jet. Jet diameter and solid volume fraction values along the jet periphery did not differ considerably for each jet, as shown in Figure 9a.

Data in Figure 12 demonstrate that the particle entrainment for a particular orifice does not necessarily increase with an increase in fluidization velocity. This phenomena was particularly evident for the interacting jet systems ($U_f/U_{mf,2D}$ = 1.57 – 1.80). However, as noted in Figure 10a, a net increase in solid circulation $\dot{m}_{x,tot} = \sum_{j=1}^{N} \dot{m}_{x,i}$ is always observed with an increase in superficial velocity.

It was also noted that no particular orifice consistently had a maximum or minimum particle entrainment rate for all fluidization velocities. Hence, the particle entrainment rates were not biased for any particular orifice location. Aforementioned observations stress the differences between the current study and single jet experiments conducted in the literature, where such phenomena could not be noticed.

Particle Properties. Figure 13 contains a comparison of volumetric circulation rate for glass 550 μm and ceramic 550 μm particles using Type A1 distributor plate. The volumetric circulation rate was calculated by dividing the respective solid circulation rate of particle types with the particle density. As observed from the plot, the circulation rate of ceramic 550 μm particles was 14–17% higher than glass 550 μm particles at $U_f/U_{mf,2D} > 1.57$. For a relatively high difference in density of the mentioned particles, the difference in volumetric circulation rate is small. As observed from Figure 11, the average horizontal particle velocity, U_{avg}, along the jet periphery was higher for glass 550 μm particles. However, the ceramic 550 μm particle test cases produced higher jet lengths than glass 550 μm test cases, as shown in Figure 14. The jet diameter was not dependent on particle properties,[56] and hence did not significantly impact the differences in the circulation rates for the aforementioned particle types. The difference in the mean solid volume fraction, ε_s, for the two particle types was not found to be significant, with the profile for glass 550 μm particles being similar to that shown in Figure 9 for ceramic 550 μm particles. The relatively low number of data points for comparison of these two particle types is due to the fluidizing nature of ceramic 550 μm particles. For higher fluidization velocities, jets for ceramic 550 μm particles bypassed the bed height and thus their jet length was not defined. At low fluidization velocities, the estimation of accurate jet diameter for ceramic 550 μm particles was not possible due to the instability of jets.

Figure 15 contains the comparison for solid circulation rate of glass 550 μm and glass 750 μm particles using Type B1 distributor plate. For glass 750 μm particles, the data was obtained for velocities both below and above its minimum fluidization velocity ($U_f/U_{mf,2D}$ = 1). For glass 550 μm particles, the solid circulation rate was obtained only for velocities greater than its minimum fluidization velocity. As observed from the plot, the solid circulation rate for glass 750 μm particles exceeded the solid circulation rate of the glass 550 μm particles at $U_f/U_{mf,2D}$ greater than 1.

A similar trend was seen when both particles were tested with the Type A1 distributor plate, as shown in Figure 10a. This plot contains the data at velocity higher than minimum fluidization ($U_f/U_{mf,2D}$ = 1) for both particle types. In this

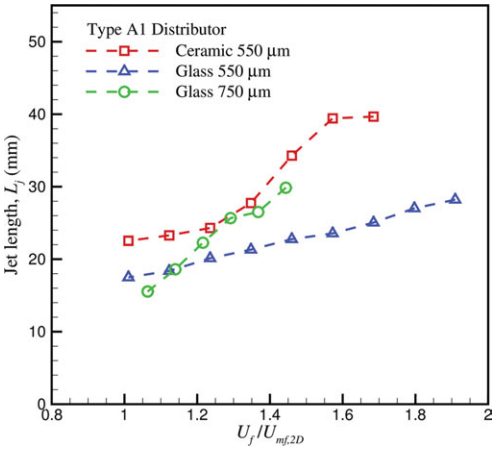

Figure 14. Jet penetration length vs. $U_f/U_{mf,2D}$ for the three particle types using Type A1 distributor plate.

[Color figure can be viewed in the online issue, which is available at wileyonlinelibrary.com.]

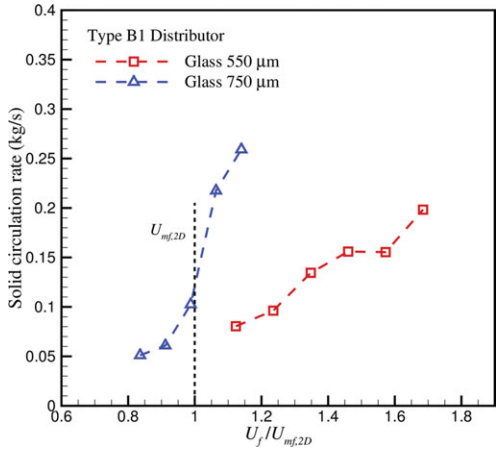

Figure 15. Solid circulation rate vs. $U_f/U_{mf,2D}$ for glass 550 μm and glass 750 μm particles using Type B1 distributor plate.

[Color figure can be viewed in the online issue, which is available at wileyonlinelibrary.com.]

comparison, again at $U_f/U_{mf,2D}$ greater than 1, the solid circulation rate for glass 750 μm particles was found to be higher than that of glass 550 μm particles. The jet penetration length for glass 750 μm particles was found to be higher than that of glass 550 μm particles, as seen from Figure 14. Also, as observed from Figure 11, the average velocity along the jet periphery, U_{avg}, was found to be higher for glass 750 μm particles.

In their respective single jet experiments, Filla et al.[18] and Kim et al.[20] noticed an increase in entrainment rate for the increase in particle diameter. Filla et al.[18] attributed both higher solid fraction values and higher entrainment velocities throughout the jet, leading to higher momentum exchange between the solids and gas, for the increase in entrainment rate for coarser particles. However, the theoretical model of Baeyens et al.[9] disagreed with this impact of particle diameter on the particle entrainment values, where it was concluded that at equal values of excess velocity ($U_f - U_{mf}$) the entrainment rate decreases for coarser particles. José et al.[27] observed an increase in solid circulation rate for the decrease in particle density, and also acknowledged that the horizontal component of particle entrainment velocity decreases with the decrease in particle density. Filla et al.[18] concluded that the resistance of the particulate phase to the dilute region of jet is larger for smaller and lighter particles, leading to lower entrainment velocities. These data agree with the findings presented in the current study.

Distributor Configuration. Distributor Type A1 and A2 were tested with glass 550 μm particles to understand the effect of the change in orifice pitch on the solid circulation rate. Figures 16a, b shows the solid circulation rate for aforementioned distributors vs. $U_f/U_{mf,2D}$ and orifice velocity, respectively. As observed from Figure 16a, the solid circulation rate of Type A2 distributor was slightly higher, if not equal, in comparison to the data for Type A1 distributor at the same $U_f/U_{mf,2D}$. Due to fewer holes in Type A2 distributor, the orifice velocity for Type A2 is calculated to be higher than Type A1 at same fluidization velocities. Hence, as observed from Figure 16b, when the solid circulation data was observed for the same orifice velocities, the solid circulation rate for Type A1 distributor was found to be higher than Type A2. The solid circulation for Type A1 distributor is much higher than Type A2 distributor due to higher average entrainment velocities, U_{avg}, and higher jet lengths[56] at the same orifice velocities. Although the particle entrainment rate measured for each jet

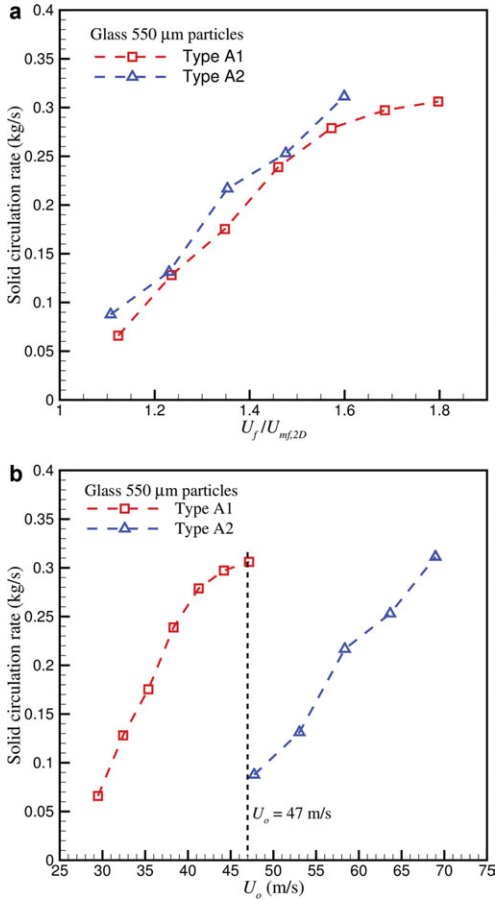

Figure 16. Comparison of solid circulation rates for Type A1 and A2 distributor plates using glass 550 μm particles.

(a) vs. $U_f/U_{mf,2D}$. (b) vs. orifice velocity. [Color figure can be viewed in the online issue, which is available at wileyonlinelibrary.com.]

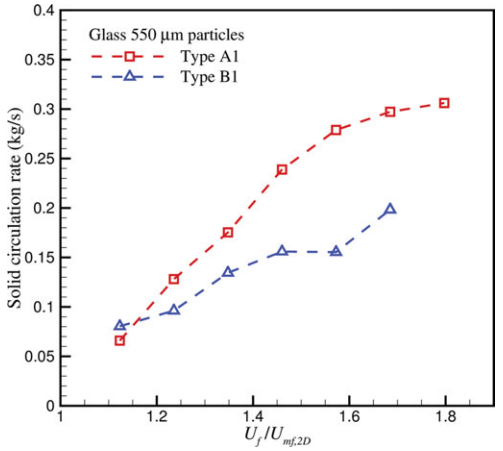

Figure 17. Solid circulation rate vs. $U_f/U_{mf,2D}$ for Type A1 and B1 distributor plates using glass 550 μm particles.

[Color figure can be viewed in the online issue, which is available at wileyonlinelibrary.com.]

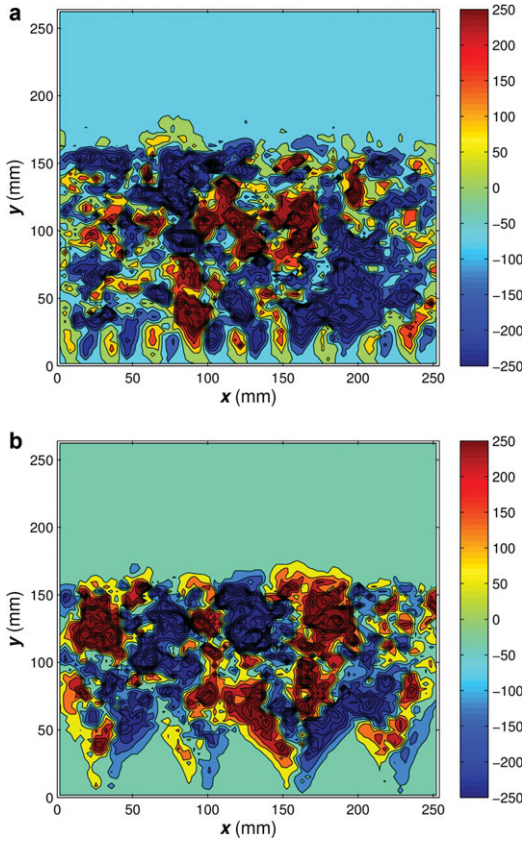

Figure 18. Comparison of horizontal particle mass flux maps, $\dot{m}''_x$, at $U_f/U_{mf,2D}$ = 1.46 using glass 550 μm particles (a) Type A1 distributor (b) Type B1 distributor.

[Color figure can be viewed in the online issue, which is available at wileyonlinelibrary.com.]

in Type A2 distributor plate was higher, the number of orifices in Type A2 was lower in comparison to Type A1 distributor plate. Therefore, the total solid circulation rate for the bed decreased for a distributor plate with higher orifice pitch when compared at the same orifice velocity.

The effect of the increase in orifice diameter on solid circulation rate was measured by testing glass 550 μm particles with distributor Types A1 and B1. Distributor Type A1 and B1 were designed to have the same total orifice flow area. Hence, at the same superficial velocity, the effect of orifice diameter can be compared at the same orifice velocity for these distributors. For Type B1 distributor, the jet penetration length[56] and particle entrainment rate per jet was found to be higher than Type A1 distributor. However, the average particle entrainment velocities and number of orifices were higher for Type A1 distributor. Figure 17 contains the solid circulation rate data for the two test cases. It should be noted from Table 3 that $U_{mf,2D}$ for both test-cases is same. As observed, the circulation rate for Type A1 distributor was measured to be 30–80% higher than Type B1 distributor plate. Hence, for a distributor plate design, the plate with large number of small diameter orifices was found to be effective at enhancing the circulation rate. This is also evident from the horizontal particle mass flux maps plotted for the two distributor plates at $U_f/U_{mf,2D}$ = 1.46 using glass 550 μm particles in Figures 18a, b. The horizontal velocity flux maps show a more uniform mixing for Type A1 distributor plate. For Type B1 distributor plate, the mixing was not existent in the regions between the adjacent jets. The difference in size of this dead zone region is responsible for higher circulation rates in Type A1 distributor plate when compared with Type A2 and B1 distributor plates.

José et al.[24] observed a decrease in circulation rate for increase in orifice diameter, similar to the results observed in the current study. However, Thorley et al.[1] reported the contrary in their experiments. It must be noted that in both studies a single jet was used. Hence, the total orifice flow area as well as the orifice velocity were not sufficient to differentiate the expected solid circulation.

The leveling off of solid circulation rate was observed to occur earlier for Type B1 distributor plate, as shown in Figure 17. At the maximum fluidization velocity ($U_f/U_{mf,2D}$ = 1.68), the effect of the jet bypassing the bed height increases the solid circulation rate for Type B1 distributor plate.

Conclusions

PIV was used to investigate the evolution of multiple inlet gas jets located at the distributor base of a two-dimensional fluidized bed setup. A correlation was developed to estimate the solid volume fraction using digital image analysis on the results. The solid volume fraction profile and PIV results were used to quantify the solid circulation rate in the fluidized bed. The effects of fluidization velocity, orifice diameter, orifice pitch, particle diameter, and particle density were studied on the solid circulation rate. The solid volume fraction model compared well with a similar model suggested by Link et al.[36,37] For all test cases, the mass of bed media estimated using this model was within 15% of the actual bed mass. The solid volume fraction profiles were similar to those observed in the literature.

Solid circulation was found to increase linearly with an increase in fluidization velocity until the jet systems transitioned from isolated jets to interacting systems. For an interacting jet system, the solid circulation increased with fluidization velocity but at a much lower rate. In a multiple jet system, this phenomenon may indicate an optimum operating condition for a bed that requires high circulation rate for low air input. The accuracy of the solid circulation rate calculated in the current experimental study was verified by the circulation rate calculated by the counter-current flow model in the literature.[8–10]

The circulation rate was observed to slightly increase with the decrease in particle density from 2500 kg/m^3 to 1079 kg/m^3 at same $U_f/U_{mf,2D}$. However, the horizontal particle entrainment velocities decreased significantly with this change. For $U_f/U_{mf,2D} > 1$, the solid circulation rate and entrainment velocities for glass 750 μm particles exceeded that of glass 550 μm particles.

At the same orifice velocities, a higher circulation rate was noted for distributors with smaller orifice pitch. At the same fluidization velocities and for distributors with different orifice diameters but the same orifice flow area, the circulation rate was noted to be much higher for distributors with smaller diameter orifices. Hence, for a distributor plate design, the plate with large number of small diameter orifices was found to enhance the solid circulation rate.

Acknowledgments

This work was supported by the Virginia Tech Institute for Critical Technology and Applied Science (ICTAS).

Notation

A = constant to convert I_{cor} to area fraction projected at front wall
A_d = area of distributor, m^2
B = constant to convert projected area fraction to ε_s
D_j = jet diameter, m
d_o = diameter of orifice in distributor plate, m
d_p = mean particle diameter, m
fr_{neg} = fraction of bed moving with a negative vertical velocity at a specific fluidization velocity
I_{cor} = corrected image intensity averaged over an interrogation area
I_m = manipulated intensity of the captured image
L_j = jet penetration length, m
$\dot{m}''_x$ = horizontal particle mass flux in the interrogation area; $= \rho_p \varepsilon_s \overrightarrow{u}$, kg/m^2 s
$\dot{m}''_y$ = vertical particle mass flux in the interrogation area; $= \rho_p \varepsilon_s \overrightarrow{v}$, kg/m^2 s
$\dot{m}_{x,j}$ = horizontal particle entrainment rate of a particular jet, kg/s
$\dot{m}_{x,tot}$ = total solid circulation rate of the bed (kg/s), $= \sum_{j=1}^{N} \dot{m}_{x,j}$
N = number of orifices within the distributor plate
P = pitch of orifices within the distributor, m
U_{avg} = average of $\overrightarrow{u}$ calculated at jet periphery for all jets in a bed at a set air flow rate
U_f = superficial gas velocity, m/s
U_{mf} = superficial gas velocity at minimum fluidization, m/s
$U_{mf,2D}$ = experimental U_{mf} of corresponding distributor plate and particle test case, m/s
$U_{mf,3D}$ = experimental minimum fluidization velocity measured in a cylindrical bed, $= U_{mf}$, m/s
U_o = mean orifice velocity (m/s), $= (U_f A_d)/N(\pi d_o^2/4)$
$\overrightarrow{u}$ = horizontal particle velocity vector in the interrogation area, m/s
$\overrightarrow{v}$ = vertical particle velocity vector in the interrogation area, m/s
$|v_{neg,avg}|$ = mean negative vertical velocity of the particles at specific fluidization velocity
x = horizontal location along the width of fluidized bed, m
y = vertical location from the distributor base, m

Greek letters

α = particle entrainment angle, °
ε_f = mean void fraction in the interrogation area along the bed thickness, $=1-\varepsilon_s$
ε_s = mean solid volume fraction in the interrogation area along the bed thickness
$\varepsilon_{s,b}$ = bulk solid volume fraction calculated along the expanded bed dimensions
ρ_p = particle density, kg/m^3

Literature Cited

1. Thorley B, Saunby JB, Mathur KB, Osberg GL. An analysis of air and solid flow in a spouted wheat bed. *Can J Chem Eng*. 1959;37:184–192.
2. Lefroy GA. The mechanics of spouted beds. *Trans Inst Chem Eng*. 1969;47:120.
3. Gidaspow D, Ettehadieh B. Fluidization in two-dimensional beds with a jet. 2. Hydrodynamic modeling. *Ind Eng Chem Fundam.* 1983;22:193–201.
4. Patrose B, Caram HS. *The mechanics of particle motion in a grid jet*. In: Klinzing GE, editor. *AIChE Symposium Series; No. 241*, Vol. 80. New York, NY: American Institute of Chemical Engineers, 1984:48–56.
5. Ettehadieh B, Gidaspow D, Lyczkowski RW. Hydrodynamics of fluidization in a semicircular bed with a jet. *AIChe J*. 1984;30:529–536.
6. Morgan Iii MH, Day JY, Littman H. Spout voidage distribution, stability and particle circulation rates in spouted beds of coarse particles—I. Theory. *Chem Eng Sci*. 1985;40:1367–1377.
7. Day JY, Morgan Iii MH, Littman H. Measurements of spout voidage distributions, particle velocities and particle circulation rates in spouted beds of coarse particles—II. Experimental verification. *Chem Eng Sci*. 1987;42:1461–1470.
8. van Deemter JJ. The counter-current flow model of a gas-solids fluidized bed. In: *Proceedings of the International Symposium on Fluidization*. Eindhoven, June 6–9, 1967:334–347.
9. Baeyens J, Geldart D. *Solids mixing*. In: Geldart D, editor. *Gas Fluidization Technology*. Chichester, New York: Wiley, 1986:97–122.
10. van Deemter JJ. *Mixing*. In: Davidson JF, Clift R, Harrison D, editors. *Fluidization*. London: Academic Press, 1985:331–354.
11. Merry JMD. Fluid and particle entrainment into vertical jets in fluidized beds. *AIChe J*. 1976;22:315–323.
12. Donsi G, Massimilla L, Colantuoni L. *The dispersion of axi-symmetric gas jets in fluidized bed*. In: Grace JR, Matsen JM, editors. *Fluidization*. New York: Plenum Press, 1980:297–304.
13. Abramovich GN. *The Theory of Turbulent Jets*. Cambridge: MIT Press, 1963.
14. Massimilla L. *Gas jets in fluidized beds*. In: Davidson JF, Clift R, Harrison D, editors. *Fluidization*. London: Academic Press, 1985:133.
15. Gidaspow D, Lin C, Seo YC. Fluidization in two-dimensional beds with a jet. 1. Experimental porosity distributions. *Ind Eng Chem Fundam*. 1983;22:187–193.
16. Luo CH, Aoki K, Uemiya S, Kojima T. Numerical modeling of a jetting fluidized bed gasifier and the comparison with the experimental data. *Fuel Process Technol*. 1998;55:193–218.
17. Horio M, Kiyota H, Muchi I. Particle movement on a perforated plate distributor of fluidized-bed. *J Chem Eng Jpn*. 1980;13:137–142.
18. Filla M, Massimilla L, Vaccaro S. Gas jets in fluidized beds: the influence of particle size, shape and density on gas and solids entrainment. *Int J Multiphase Flow*. 1983;9:259–267.
19. Freychet N, Briens CL, Bergougnou MA, Large JF. A new approach to jet phenomena gas entrainment and recirculation in a bidimensional spouted fluidized bed. *Can J Chem Eng*. 1989;67:191–199.
20. Kim S, Cho S. Particle velocity and circulation rate in liquid spouted beds. *Korean J Chem Eng*. 1991;8:131–136.
21. Yang W-C, Keairns DL. Solid entrainment rate into gas and gas–solid, two-phase jets in a fluidized bed. *Powder Technol*. 1982;33:89–94.
22. Benkrid A, Caram HS. Solid flow in the annular region of a spouted bed. *AIChe J*. 1989;35:1328–1336.
23. Uemaki O, Tsuji T. Particle velocity and solids circulation rate in a jet-spouted bed. *Can J Chem Eng*. 1992;70:925–929.
24. San José MJ, Olazar M, Alvarez S, Izquierdo MA, Bilbao J. Solid cross-flow into the spout and particle trajectories in conical spouted beds. *Chem Eng Sci*. 1998;53:3561–3570.
25. Olazar M, San José MJ, Alvarez S, Morales A, Bilbao J. Measurement of particle velocities in conical spouted beds using an optical fiber probe. *Ind Eng Chem Res*. 1998;37:4520–4527.
26. Pianarosa DL, Freitas LAP, Lim CJ, Grace JR, Dogan OM. Voidage and particle velocity profiles in a spout-fluid bed. *Can J Chem Eng*. 2000;78:132–142.
27. San José MJ, Alvarez S, Morales A, Olazar M, Bilbao J. Solid cross-flow into the spout and particle trajectories in conical spouted beds consisting of solids of different density and shape. *Chem Eng Res Des*. 2006;84:487–494.
28. Kececioglu I, Yang W-C, Keairns DL. Fate of solids fed pneumatically through a jet into a fluidized bed. *AIChe J*. 1984;30:99–110.
29. Kececioglu I, Keairns DL. Computation of solid circulation rates in a fluidized bed from tracer particle concentration distributions. *Can J Chem Eng*. 1989;67:290–300.
30. Hulet C, Briens C, Berruti F, Chan EW. Effect of a shroud on entrainment into a submerged jet within a fluidized bed. *Chem Eng Process: Process Intens*. 2008;47:1435–1450.
31. Seo YC, Gidaspow D. An x-ray-.gamma.-ray method of measurement of binary solids concentrations and voids in fluidized beds. *Ind Eng Chem Res*. 1987;26:1622–1628.
32. Stein M, Seville JPK, Parker DJ. Attrition of porous glass particles in a fluidised bed. *Powder Technol*. 1998;100:242–250.
33. Yee SW. Particle motion in relatively thin fluidised bed models. *Chem Eng Sci*. 2006;61:6234–6238.
34. Chen L, Weinstein H. Shape and extent of the void formed by a horizontal jet in a fluidized bed. *AIChE J*. 1993;39:1901–1909.
35. Franka NP, Heindel TJ. Local time-averaged gas holdup in a fluidized bed with side air injection using X-ray computed tomography. *Powder Technol*. 2009;193:69–78.
36. Link J, Zeilstra C, Deen N, Kuipers H. Validation of a discrete particle model in a 2D spout-fluid bed using non-intrusive optical measuring techniques. *Can J Chem Eng*. 2004;82:30–36.
37. Link JM, Cuypers LA, Deen NG, Kuipers JAM. Flow regimes in a spout-fluid bed: a combined experimental and simulation study. *Chem Eng Sci*. 2005;60:3425–3442.

38. Laverman JA, Roghair I, Annaland MV, Kuipers H. Investigation into the hydrodynamics of gas-solid fluidized beds using particle image velocimetry coupled with digital image analysis. *Can J Chem Eng*. 2008;86:523–535.
39. van Buijtenen MS, Börner M, Deen NG, Heinrich S, Antonyuk S, Kuipers JAM. An experimental study of the effect of collision properties on spout fluidized bed dynamics. *Powder Technol*. 2011;206:139–148.
40. Liu GQ, Li SQ, Zhao XL, Yao Q. Experimental studies of particle flow dynamics in a two-dimensional spouted bed. *Chem Eng Sci*. 2008;63:1131–1141.
41. Gryczka O, Heinrich S, Miteva V, Deen NG, Kuipers JAM, Jacob M, Mörl L. Characterization of the pneumatic behavior of a novel spouted bed apparatus with two adjustable gas inlets. *Chem Eng Sci*. 2008;63:791–814.
42. Grace JR. *Agricola aground: characterization and interpretation of fluidization phenomena*. In: Weimer AW, editor. *AIChE Symposium Series*; no. 289, Vol 88. New York, NY: American Institute of Chemical Engineers, 1992:1–16.
43. Grace JR, Li T. Complementarity of CFD, experimentation and reactor models for solving challenging fluidization problems. *Particuology*. 2010;8:498–500.
44. Knowlton TM, Hirsan I. *Fluidization*. In: Grace JR, Matsen JM, editors. *International Fluidization, Conference*. New York: Plenum Press, 1980:315.
45. Hong RY, Guo QJ, Luo GH, Zhang JY, Ding J. On the jet penetration height in fluidized beds with two vertical jets. *Powder Technol*. 2003;133:216–227.
46. Ruoyo H, Hongzhong L, Maoyu C, Jiyu Z. Numerical simulation and verification of a gas-solid jet fluidized bed. *Powder Technology*. 1996;87:73–81.
47. Guo Q, Yue G, Zhang J, Liu Z. Hydrodynamic characteristics of a two-dimensional jetting fluidized bed with binary mixtures. *Chem Eng Sci*. 2001;56:4685–4694.
48. Guo QJ, Yue GX, Liu ZY. Gas discharge patterns in a large jetting fluidized bed with a vertical nozzle. *Ind Eng Chem Res*. 2001;40:3689–3696.
49. Zhang K, Zhang H, Lovick J, Zhang JY, Zhang BJ. Numerical computation and experimental verification of the jet region in a fluidized bed. *Ind Eng Chem Res*. 2002;41:3696–3704.
50. Tsukada M, Horio M. Gas motion and bubble formation at the distributor of a fluidized bed. *Powder Technol*. 1990;63:69–74.
51. Chodak J. Pyrolysis and hydrodynamics of fluidized bed media, 2010. Available at http://scholar.lib.vt.edu/theses/available/etd-05172010–091509/.
52. Poletto M, Bai R, Joseph DD. Propagation of voidage waves in a two-dimensional liquid-fluidized bed. *Int J Multiphase Flow*. 1995;21:223–239.
53. Boerefijn R, Ghadiri M. High speed video image analysis of flow of fine particles in fluidized bed jets. *Adv Powder Technol*. 1998;9:229–243.
54. Goldschmidt MJV, Link JM, Mellema S, Kuipers JAM. Digital image analysis measurements of bed expansion and segregation dynamics in dense gas-fluidised beds. *Powder Technol*. 2003;138:135–159.
55. Heffels C, Willemse A, Scarlett B. Possibilities of near backward light scattering for characterizing dense particle systems. *Powder Technol*. 1996;86:127–135.
56. Agarwal G, Lattimer B, Ekkad S, Vandsburger U. Influence of multiple gas inlet jets on fluidized bed hydrodynamics using particle image velocimetry and digital image analysis. *Powder Technol*. 2011;214:122–134.
57. Rees AC, Davidson JF, Dennis JS, et al. The nature of the flow just above the perforated plate distributor of a gas-fluidised bed, as imaged using magnetic resonance. *Chem Eng Sci*. 2006;61:6002–6015.
58. Grace JR, Lim CJ. Permanent jet formation in beds of particulate solids. *Can J Chem Eng*. 1987;65:160–162.
59. Rowe PN, Macgillivray HJ, Cheesman DJ. Gas-discharge from an orifice into a gas-fluidized bed. *Trans Inst Chem Eng*. 1979;57:194–199.
60. Pore M, Holland DJ, Chandrasekera TC, et al. Magnetic resonance studies of a gas-solids fluidised bed: jet-jet and jet-wall interactions. *Particuology*. 2010;8:617–622.
61. Dong S, Cao C, Si C, Guo Q. Effect of perforated ratios of distributor on the fluidization characteristics in a gas–solid fluidized bed. *Ind Eng Chem Res*. 2008;48:517–527.
62. Geldart D. *Gas Fluidization Technology*. New York: Wiley, 1986.
63. Kunii D, Levenspiel O. *Fluidization Engineering*. Boston: Butterworth-Heinemann, 1991.
64. Santana D, Nauri S, Acosta A, Garcia N, Macias-Machin A. Initial particle velocity spatial distribution from 2-D erupting bubbles in fluidized beds. *Powder Technol*. 2005;150:1–8.
65. Muller CR, Davidson JF, Dennis JS, Hayhurst AN. A study of the motion and eruption of a bubble at the surface of a two-dimensional fluidized bed using particle image velocimetry (PIV). *Ind Eng Chem Res*. 2007;46:1642–1652.

Manuscript received July 15, 2011, and revision received Oct. 12, 2011.